10

A New Systemic Study Regarding the Behaviour of Some Alloy Steels During Low Cycles Fatigue Process

Macuta Silviu
Dunarea de Jos University of Galati
Romania

1. Introduction

The research of the metallic materials used in machine manufacturing to which high stress and a small number of cycles is applied have been increasingly gained interest in the last 40 years; this is because during cyclical stress at critical points in terms of resistance repeated strain occurs in many major constructions.

Fatigue breaking to a small number of cycles and high strains is encountered in the operation of various types of machines: power machine, elements of heating boilers or heat exchangers in electro nuclear industry, pressure vessels, steam and hydro turbines, turbo compressors, the plane landing trains and other transport means and mechanisms.

The process of cracking and breaking by fatigue is characterized by different mechanisms at different levels of strain. Thus Wöhler's curve can be studied in 3 areas:

The first area called the quasi-static field, where $N=0\div10^4$ cycles, when there are large plastic strains;

The second area called the area of limited durability, where $N=10^4\div10\cdot10^6$ cycles, breaking in this situation implies elastoplastic strain and calculations will be carried out to limited durability.

The third area - the area of unlimited durability, or the fatigue resistance range, when $N>10\cdot10^6$ cycles. Breaking is characterized by elastic strain only.

Regarding the first area, a more careful research led to the conclusion that there are two distinct zones:

The quasi-static area itself, for $N<10^3$ cycles - area where high strains close to the material yielding point occur, where breaking is characterized by large plastic strain, similar to static fracture.

The low-cycle fatigue zone also called the *low cycle fatigue* where $N=5\cdot10^2\div10^4$ cycles, where this time breaking is characterized by elastoplastic strain. A deeper insight into this area has revealed the existence of anomalies (discontinuities) of the fatigue curve. The problem was first studied by R. Moore in 1923, then by Sabolin, Finney and Mann .

The phenomenon of fatigue to a small number of cycles has three specific features.

1. High level of strains
2. Low testing time (10^3-10^4, max. 10^5 cycles)
3. Reduced testing frequency(up to50 cycles/min)

Investigating the low cycle fatigue damage, it can be distinguished between a rigid and a soft loading regime.

The studies carried out have a general character, the fatigue behaviour being determined from the fatigue curves, the curves of mechanical hysteresis and the cyclic cold-hardening curves. Based on the investigations, a set of rules and criteria to predict the material behaviour to *low cycle* strains has been established.

2. A new systemic approach of the fatigued surface layer behavior

The concept of a *structural cybernetic pattern* has been introduced in order to obtain an as complete as possible approach of the surface layer behavior and also with a view to analyzing and emphasizing the main factors and parameters which determine the fatigue process. This concept, introduced by professor I. Crudu from Dunarea de Jos University of Galati-Romania in order to characterize a tribosystem, was extended to the characterization of the fatigued surface layer and it represents a totally new approach of the fatigue process.

In this chapter a new research methodology has been developed along with a way to approach the fatigue behaviour of the surface layer to high strains and small number of cycles by extending the concept of structural cybernetic tribo-system.

For the research purpose, special equipment was needed consisting of a patented Universal Machine for fatigue testings and related facilities. The development of certain surface layer parameters was monitored (1st and 2nd order strains, dislocation density, crystalline lattice parameter, texture, microstructure, and micro-hardness of the surface layer) during the fatigue process according to the control parameter (number cycles, strain, frequency, type of material required).

In order to have an as extensively as possible approach to the surface layer behavior and to track and highlight the main factors and parameters determining the process of destruction by fatigue, the concept of *structural cybernetic model* was introduced. This concept was introduced to characterize a tribosystem and allowed its extension to the characterization of the surface layer of the material subject to fatigue, which is an entirely new approach to fatigue processes.

Fig. 1 shows a structural cybernetic model by means of which the changes of the input parameters can be systematically monitored by measuring the output parameters of the surface layer undergoing the action of destruction by fatigue.

The input-output parameters of the cybernetic model include the parameters of the surface layer ($(S_s$-$S'_s)$ and the control parameters (U). Surface layer parameters can be grouped into:

geometric parameters (macro-geometry and micro-geometry- X_1- X'_1)

mechanical parameters (hardness and micro hardness – X_2 -X'_2 and the strain state – X_3- X'_3);

physical and metallurgical parameters (chemical composition – X_4- X'_4, structure – X_5- X'_5, purity – X_6- X'_6)..

Some of these parameters, such as micro hardness - X_2, strain - and structure X_3 - X_5, may be modified from outside so that the life time of a material under fatigue process can be modified within certain limits, as desired.

The control parameters (U) also called external factors are those parameters which by their action on the functioning of the fatigue testing machine may modify some parameters of the surface layer of the material the test-piece is made of. The control parameters can be grouped into:

Constructive parameters (nature of the material - U_1, test-piece shape - U_2, the test-piece dimensions - U_3);

Operating parameters (working environment - U4, cinematic - U5 and energy parameters - U6).

Under the experimental program, out of all surface layer parameters, the evolution with respect to the initial state (input parameters) of the following parameters (output parameters) has been investigated: mechanical parameters (micro hardness - X2; state of strain - X3 namely: 1st order strain (σ_I) - X_3^1,) -2nd order strain (σ_{II}) - X_3^2 ; -,3rd order strain ((ρ) - X_3^3, - and from the physical metallurgical parameters, the structure changes were monitored - X5 (network parameters, the texture).

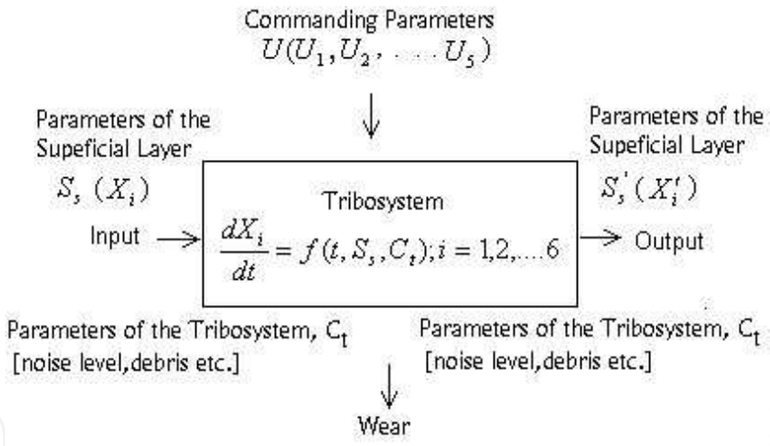

Fig. 1. A cybernetic model used in study of friction process adapted in study of the low cycle fatigue process.

From among the control parameters (U), for the purpose of the experiment, the constructive parameter was acted upon by the nature of the material U1, using two grades of steel OL52 and 10TiNiCr180, both shape and dimensions of the test pieces remaining unchanged throughout the experiment. From among the operating parameters, it was maintained the same working environment - air at ambient temperature (U4), acting upon the cinematic parameters U_5, namely the testing frequency ν_1= 20 cycles / min or ν_2= 40 cycles / min

It was also acted upon the energy parameters (U6),in an attempt to investigate the evolution of the surface layer parameters by changing the imposed strains (ε_1, ε_2, ε_3)) and the number of strain cycles (N1, N2, N3, N4, N5) under an experimental program.

Knowing at any time the parameters of the surface layer, this is one of the safest procedures in assessing and forecasting the degree of degradation of metallic materials under fatigue processes .

Determination of the structural changes in the surface layers may allow for the optimization of the metal components manufacturing technology. In practice the control of the surface layer parameters often requires the use of physical methods of investigation which do not affect its structure and physical-chemical condition.

3. Experimental researches

This chapter presents only the experimental research carried out for the steel OL52. The experimental research was performed in steps from 2000 to 2000 cycles up to 10^4 cycles.

At each step of the number of cycles (2000 cycles) investigations were carried out on the evolution of the crystalline network parameter, trap, density, texture, analysis of the micro hardness and the evolution of the layer micro-structure. For all these investigations use was made of a diffractometer of X radiation, DRON-3, micro hardness meter PMT3, and optical microscope Olympus BX60M of Japanese construction.

Mention must be made that there has not been made a systematic research of the surface layer for the following reasons: wide variety of materials, wide range of physical, chemical, mechanical and metallurgical factors influencing on the surface layer, various deficient physical methods of non-destructive control. The relatively long time taken for some of the analyzing methods as compared to the stress relaxation period/time of certain structure modifications, gets in the way of finding a common point of view on and general methods for analyzing and controlling the different processes occurred in the surface layer.

The experimental program consists of:

Experiment 1 – carbon steel sample OL52 under stress at frequency ν_1=20 cycles/min;

Experiment 2 – carbon steel sample OL52 under stress at frequency ν_2=40 cycles/min;

Experiment 3 – alloyed steel sample 10TiNiCr180 under stress at frequency ν_1=20 cycles/min;

Experiment 4 –alloyed steel sample 10TiNiCr180 under stress at frequency ν_2=40 cycles/min;

All the 4 experiments were focused on the modifications of the surface layer parameters depending on the number of cycles N_1, N_2, N_3, N_4, N_5 and the prescribed deformations ε_1, ε_2, ε_3.

Tables 1, 2, 3, 4 illustrates the experimental program, highlighting all the parameters involved in the experiment.

TEST PROGRAM (Tables 1,2)

OAL_{ji}, $1AL_{ji}$ - A(OL52) steel samples at two stress frequencies $\sigma_{I\ i,j,k}$ – Ist order stress $a_{i,j,k}$ - lattice parameter ε_j – induced deformations, (j=1...3). $\sigma_{II\ i,j,k}$ – IInd order stress $texture_{i,j,k}$ N_k – number of stress cycles, (k=1...5).$\rho_{i,j,k}$ – displacement density, $HV_{i,j,k}$ – micro-hardness

TEST 1																
OL52 steel - frequency ν_1=20 cycles/min																
OAL_{11}	ε_1 [μm/m]					OAL_{21}	ε_2 [μm/m]					OAL_{31}	ε_3 [μm/m]				
	N_1	N_2	N_3	N_4	N_5		N_1	N_2	N_3	N_4	N_5		N_1	N_2	N_3	N_4	N_5
	$\sigma_{I\,i,j,k}$; $\sigma_{II\,i,j,k}$; $\rho_{i,j,k}$; $a_{i,j,k}$; texture, micro-hardness $HV_{i,j,k}$						$\sigma_{I\,i,j,k}$; $\sigma_{II\,i,j,k}$; $\rho_{i,j,k}$; $a_{i,j,k}$; texture, micro-hardness $HV_{i,j,k}$						$\sigma_{I\,i,j,k}$; $\sigma_{II\,i,j,k}$; $\rho_{i,j,k}$; $a_{i,j,k}$; texture, micro-hardness $HV_{i,j,k}$				
OAL_{12}	ε_1 [μm/m]					OAL_{22}	ε_2 [μm/m]					OAL_{32}	ε_3 [μm/m]				
	N_1	N_2	N_3	N_4	N_5		N_1	N_2	N_3	N_4	N_5		N_1	N_2	N_3	N_4	N_5
	surface layer properties $\sigma_{I\,i,j,k}$; $\sigma_{II\,i,j,k}$; $\rho_{i,j,k}$; $a_{i,j,k}$; texture, micro-hardness $HV_{i,j,k}$						surface layer properties $\sigma_{I\,i,j,k}$; $\sigma_{II\,i,j,k}$; $\rho_{i,j,k}$; $a_{i,j,k}$; texture, micro-hardness $HV_{i,j,k}$						surface layer properties $\sigma_{I\,i,j,k}$; $\sigma_{II\,i,j,k}$; $\rho_{i,j,k}$; $a_{i,j,k}$; texture, micro-hardness $HV_{i,j,k}$				
OAL_{13}	ε_1 [μm/m]					OAL_{23}	ε_2 [μm/m]					OAL_{33}	ε_3 [μm/m]				
	N_1	N_2	N_3	N_4	N_5		N_1	N_2	N_3	N_4	N_5		N_1	N_2	N_3	N_4	N_5
	$\sigma_{I\,i,j,k}$; $\sigma_{II\,i,j,k}$; $\rho_{i,j,k}$; $a_{i,j,k}$; texture, micro-hardness $HV_{i,j,k}$						$\sigma_{I\,i,j,k}$; $\sigma_{II\,i,j,k}$; $\rho_{i,j,k}$; $a_{i,j,k}$; texture, micro-hardness $HV_{i,j,k}$						$\sigma_{I\,i,j,k}$; $\sigma_{II\,i,j,k}$; $\rho_{i,j,k}$; $a_{i,j,k}$; texture, micro-hardness $HV_{i,j,k}$				

Table 1. Test program for OL52 steel - frequency ν_1=20 cycles/min

TEST 2																
OL52 steel - frequency ν_1=40 cycles/min																
$1AL_{11}$	ε_1 [μm/m]					AL_{21}	ε_2 [μm/m]					$1AL_{31}$	ε_3 [μm/m]				
	N_1	N_2	N_3	N_4	N_5		N_1	N_2	N_3	N_4	N_5		N_1	N_2	N_3	N_4	N_5
	$\sigma_{I\,i,j,k}$; $\sigma_{II\,i,j,k}$; $\rho_{i,j,k}$; $a_{i,j,k}$; texture, micro-hardness $HV_{i,j,k}$						$\sigma_{I\,i,j,k}$; $\sigma_{II\,i,j,k}$; $\rho_{i,j,k}$; $a_{i,j,k}$; texture, micro-hardness $HV_{i,j,k}$						$\sigma_{I\,i,j,k}$; $\sigma_{II\,i,j,k}$; $\rho_{i,j,k}$; $a_{i,j,k}$; texture, micro-hardness $HV_{i,j,k}$				
$1AL_{12}$	ε_1 [μm/m]					$1AL_{22}$	ε_2 [μm/m]					$1AL_{32}$	ε_3 [μm/m]				
	N_1	N_2	N_3	N_4	N_5		N_1	N_2	N_3	N_4	N_5		N_1	N_2	N_3	N_4	N_5
	$\sigma_{I\,i,j,k}$; $\sigma_{II\,i,j,k}$; $\rho_{i,j,k}$; $a_{i,j,k}$; texture, micro-hardness $HV_{i,j,k}$						$\sigma_{I\,i,j,k}$; $\sigma_{II\,i,j,k}$; $\rho_{i,j,k}$; $a_{i,j,k}$; texture, micro-hardness $HV_{i,j,k}$						$\sigma_{I\,i,j,k}$; $\sigma_{II\,i,j,k}$; $\rho_{i,j,k}$; $a_{i,j,k}$; texture, micro-hardness $HV_{i,j,k}$				
$1AL_{13}$	ε_1 [μm/m]					$1AL_{23}$	ε_2 [μm/m]					$1AL_{33}$	ε_3 [μm/m]				
	N_1	N_2	N_3	N_4	N_5		N_1	N_2	N_3	N_4	N_5		N_1	N_2	N_3	N_4	N_5
	$\sigma_{I\,i,j,k}$; $\sigma_{II\,i,j,k}$; $\rho_{i,j,k}$; $a_{i,j,k}$; texture, micro-hardness $HV_{i,j,k}$						$\sigma_{I\,i,j,k}$; $\sigma_{II\,i,j,k}$; $\rho_{i,j,k}$; $a_{i,j,k}$; texture, micro-hardness $HV_{i,j,k}$						$\sigma_{I\,i,j,k}$; $\sigma_{II\,i,j,k}$; $\rho_{i,j,k}$; $a_{i,j,k}$; texture, micro-hardness $HV_{i,j,k}$				

Table 2. Test program for OL52 steel - frequency ν1=40 cycles/min

TEST 3															
10TiNiCr180 alloy steel - frequency ν_1=20 cycles/min															
OBL_{11}	ε_1 [μm/m]					OBL_{21}	ε_2 [μm/m]					OBL_{31}	ε_3 [μm/m]				
	N_1	N_2	N_3	N_4	N_5		N_1	N_2	N_3	N_4	N_5		N_1	N_2	N_3	N_4	N_5
	$\sigma_{I\,i,j,k}$; $\sigma_{II\,i,j,k}$; $\rho_{i,j,k}$; $a_{i,j,k}$; texture, micro-hardness $HV_{i,j,k}$						$\sigma_{I\,i,j,k}$; $\sigma_{II\,i,j,k}$; $\rho_{i,j,k}$; $a_{i,j,k}$; texture, micro-hardness $HV_{i,j,k}$						$\sigma_{I\,i,j,k}$; $\sigma_{II\,i,j,k}$; $\rho_{i,j,k}$; $a_{i,j,k}$; texture, micro-hardness $HV_{i,j,k}$				
OBL_{12}	ε_1 [μm/m]					OBL_{22}	ε_2 [μm/m]					OBL_{32}	ε_3 [μm/m]				
	N_1	N_2	N_3	N_4	N_5		N_1	N_2	N_3	N_4	N_5		N_1	N_2	N_3	N_4	N_5
	surface layer properties $\sigma_{I\,i,j,k}$; $\sigma_{II\,i,j,k}$; $\rho_{i,j,k}$; $a_{i,j,k}$; texture, micro-hardness $HV_{i,j,k}$						surface layer properties $\sigma_{I\,i,j,k}$; $\sigma_{II\,i,j,k}$; $\rho_{i,j,k}$; $a_{i,j,k}$; texture, micro-hardness $HV_{i,j,k}$						surface layer properties $\sigma_{I\,i,j,k}$; $\sigma_{II\,i,j,k}$; $\rho_{i,j,k}$; $a_{i,j,k}$; texture, micro-hardness $HV_{i,j,k}$				
OBL_{13}	ε_1 [μm/m]					OBL_{23}	ε_2 [μm/m]					OBL_{33}	ε_3 [μm/m]				
	N_1	N_2	N_3	N_4	N_5		N_1	N_2	N_3	N_4	N_5		N_1	N_2	N_3	N_4	N_5
	$\sigma_{I\,i,j,k}$; $\sigma_{II\,i,j,k}$; $\rho_{i,j,k}$; $a_{i,j,k}$; texture, micro-hardness $HV_{i,j,k}$						$\sigma_{I\,i,j,k}$; $\sigma_{II\,i,j,k}$; $\rho_{i,j,k}$; $a_{i,j,k}$; texture, micro-hardness $HV_{i,j,k}$						$\sigma_{I\,i,j,k}$; $\sigma_{II\,i,j,k}$; $\rho_{i,j,k}$; $a_{i,j,k}$; texture, micro-hardness $HV_{i,j,k}$				

Table 3. Test program for 10TiNiCr180 alloy steel - frequency ν_1=20 cycles/min

TEST 4															
10TiNiCr180 alloy steel - frequency ν_2=40 cycles/min															
$1BL_{11}$	ε_1 [μm/m]					$1BL_{21}$	ε_2 [μm/m]					$1BL_{31}$	ε_3 [μm/m]				
	N_1	N_2	N_3	N_4	N_5		N_1	N_2	N_3	N_4	N_5		N_1	N_2	N_3	N_4	N_5
	$\sigma_{I\,i,j,k}$; $\sigma_{II\,i,j,k}$; $\rho_{i,j,k}$; $a_{i,j,k}$; texture, micro-hardness $HV_{i,j,k}$						$\sigma_{I\,i,j,k}$; $\sigma_{II\,i,j,k}$; $\rho_{i,j,k}$; $a_{i,j,k}$; texture, micro-hardness $HV_{i,j,k}$						$\sigma_{I\,i,j,k}$; $\sigma_{II\,i,j,k}$; $\rho_{i,j,k}$; $a_{i,j,k}$; texture, micro-hardness $HV_{i,j,k}$				
$1BL_{12}$	ε_1 [μm/m]					$1BL_{22}$	ε_2 [μm/m]					$1BL_{32}$	ε_3 [μm/m]				
	N_1	N_2	N_3	N_4	N_5		N_1	N_2	N_3	N_4	N_5		N_1	N_2	N_3	N_4	N_5
	$\sigma_{I\,i,j,k}$; $\sigma_{II\,i,j,k}$; $\rho_{i,j,k}$; $a_{i,j,k}$; texture, micro-hardness $HV_{i,j,k}$						$\sigma_{I\,i,j,k}$; $\sigma_{II\,i,j,k}$; $\rho_{i,j,k}$; $a_{i,j,k}$; texture, micro-hardness $HV_{i,j,k}$						$\sigma_{I\,i,j,k}$; $\sigma_{II\,i,j,k}$; $\rho_{i,j,k}$; $a_{i,j,k}$; texture, micro-hardness $HV_{i,j,k}$				
$1BL_{13}$	ε_1 [μm/m]					$1BL_{23}$	ε_2 [μm/m]					$1BL_{33}$	ε_3 [μm/m]				
	N_1	N_2	N_3	N_4	N_5		N_1	N_2	N_3	N_4	N_5		N_1	N_2	N_3	N_4	N_5
	$\sigma_{I\,i,j,k}$; $\sigma_{II\,i,j,k}$; $\rho_{i,j,k}$; $a_{i,j,k}$; texture, micro-hardness $HV_{i,j,k}$						$\sigma_{I\,i,j,k}$; $\sigma_{II\,i,j,k}$; $\rho_{i,j,k}$; $a_{i,j,k}$; texture, micro-hardness $HV_{i,j,k}$						$\sigma_{I\,i,j,k}$; $\sigma_{II\,i,j,k}$; $\rho_{i,j,k}$; $a_{i,j,k}$; texture, micro-hardness $HV_{i,j,k}$				

Table 4. Test program for 10TiNiCr180 alloy steel - frequency ν_2=40 cycles/min

TEST PROGRAM

$0BL_{ji}$, $1BL_{ji}$ - B (10TiNiCr180) steel samples at two stress frequencies $\sigma_{I\,i,j,k}$ – Ist order stress a $_{i,j,k}$ - lattice parameter ε_j – induced deformations, (j=1...3).$\sigma_{II\,i,j,k}$ – IInd order stress texture$_{i,j,k}$

N_k – number of stress cycles, (k=1...5).$\rho_{i,j,k}$ – displacement density $HV_{i,j,k}$ – micro-hardness

3.1 Sample preparation

The samples have been prepared metallographically according to the standards in force. The metallographic analysis has been made on samples from the two steel grades investigated. Samples have been taken longitudinally and investigated at a size of (x100). For purity purpose samples have been prepared and analyzed acc to [121], and for microstructure and grain size acc. to STAS 7626-79, STAS 5490-80 and SR ISO 643-93 [120].

The attack for the sample made from OL 52 was achieved by means of the natal reactant , 2% and for the sample made from TiNiCr180 with nitrogen acid reactant, 50% under electrolytic attack regime. Results are given in table 5 and 6.

Material	Purity STAS 5949-80	Microstructures STAS 7626-79 and SR ISO 643-93	Figures
OL52	Silicates + punctilious oxides score>5	Ferrite + perlite Grain size = 9 Ratio Pe/Fe=15/85	2, 3
10TiNiCr180	Titanium nitrure score=2,5	Austenitic structure with **maclați** grains and chrome carbides distributed in rows; M:G:=4-5	4 5

Table 5. Initial result for samples

In order to closely watch any microstructure modifications with the samples coded OAL_{ji}, $1AL_{ji}$, OBL_{ji} and $1BL_{ji}$, surface micro-photos were taken at size (x200, x500, x1000) directly on the samples subject to strain.

Due to the big sample sizes, vs an optimum size of a metallographic slif , it was rather difficult to prepare the surface being investigated .

The samples not chemically attacked by reactants were photographed at size (x100), and those attacked at (x200, x500, x1000).

Since the samples made from alloyed steel (austenitic stainless steel strongly anti-corrosive) are of bigger size, they have been immersed into the reactant for 30 min. The chemical composition of the reactant was: nitrogen acid (1,4) 5 ml, fluoride acid 1 ml, distilled water 44 ml, and for the carbon steel , the reactant was inital 2%.

In order to adjust the machine to 3 prescribed deformations, acc to another experimental program, captor-samples were prepared.

sample	Structure	Notifications
Şlif 1 Carbon steel	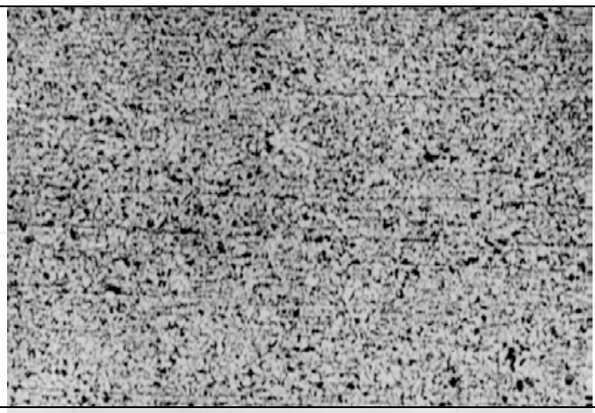	Fig. 2. Ferrite-perlitic microstructure OL52x100 grain size = 9 ratio Pe/Fe=15/85 natal attack 2%
Şlif 2 oțel carbon	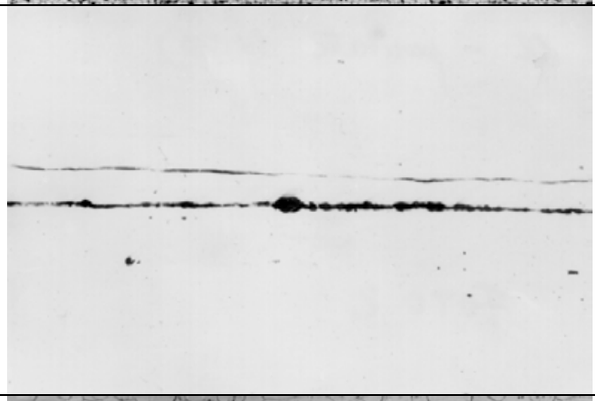	Fig. 3. OL52x100 purity – nonmetallic inclusions fragile silicates - punctilios oxides- score > 5
Şlif 3 Alloyed steel	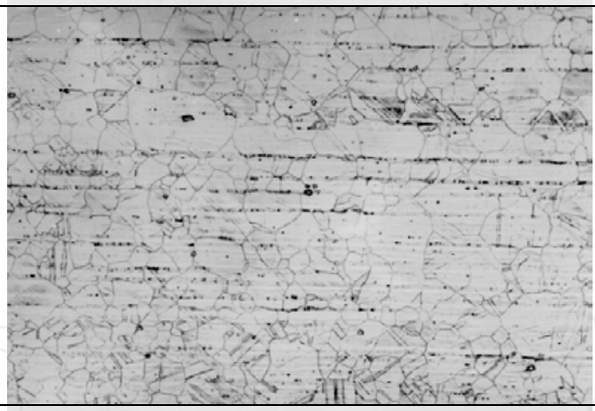	Fig. 4. Austenitic microstructure 10TiNiCr180x100
Şlif 4 Alloyed steel	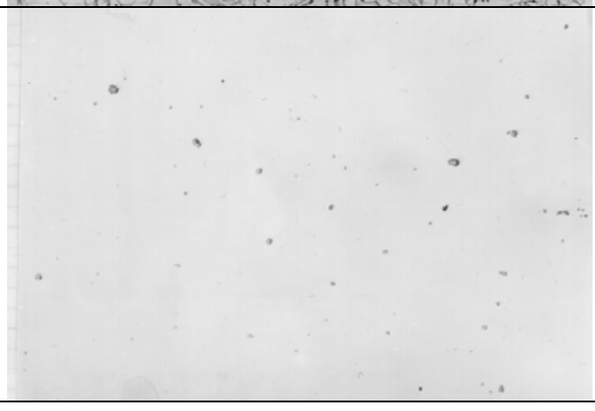	Fig. 5. 10TiNiCr180x100

3.2 Determination of the prescribed deformations

In order to determine the upper limit of the conventional elastic range, and to assess the prescribed deformations used for the experiment purpose an experimental program was designed consisting of :

1. preparation of the captor-samples
2. analysis of the captor –samples operation
3. partial plotting of the characteristic curves for the two materials specifying the prescribed deformations
4. experimental determination of the longitudinal elastic module and max strains.

Preparing the captor-samples

The samples were marked to facilitate identification:

the samples from material A (OL52) was marked 2.1, 2.2, 2.3 acc to the three prescribed deformations to be used in the experiment, and those from material B (10TiNiCr180) marked 1.1, 1.2,1.3. In the central measuring zone, on both sides a mechanical processing of the surfaces with abrasive paper to achieve the desired roughness : 1.5 … 2 μm.

After this processing the cross sections were measured and the results given in Table 6 (fig 6).

sample Dimensions [mm]	1.1	1.2	1.3	2.1	2.2	2.3
b	10.16	10.17	10.17	10.13	9.35	10.05
h	4.78	4.85	4.60	4.25	4.35	4.60

Table 6. Sample dimensions

The processed surfaces were marked (the middle of the surface was plotted on both directions) and subsequently chemically prepared .The chemical preparation involves degreasing with **dicloretan** and carbon **tetraclorură**, with a number of flushes in **isopropilic** alcohol. The adhesive used to stick the marks was "Z70" - Hottinger, a fast-hardening cyanoacrylate. For an even as possible hardness over the entire surface of the mark (without polimerisation poles) a neutralizing solution "NZ70" Hottinger was resorted to

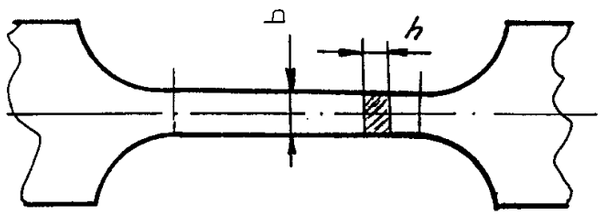

Fig. 6. Captor sample

The tensometric marks were of the type: 3P/120LY11 made by Hottinger with constant k=2.04 ±1%. The complex mark-adhesive and coating was chosen depending on the degree of compliance with the rule of the dissipated power over tensometric mark. The dissipated power on the grill surface is calculated

Two grades of rolled steels mainly used in pressure boilers and vessels industry, namely, OL52k and austenite alloyed steel 10TiNiCr180, were considered. Samples made from the above mentioned steels were tested on the universal machine at 50 tf hydraulically-driven pull at the department of material strength, the Faculty of Mechanical Engineering Galati.

On the same machine pure bending testings were conducted by making use of a construction illustrated in figure 7.

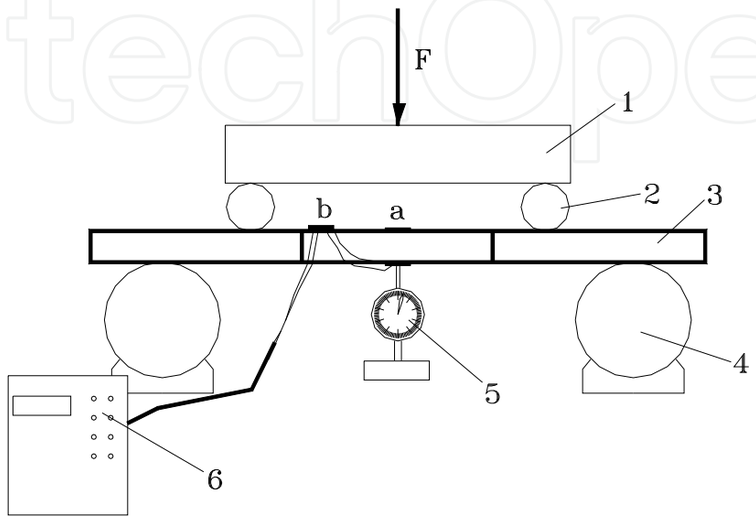

Fig. 7. The construction used for pure bending testings, were: 1 - plate, 2 - roller, 3 - sample, 4 - base roller, 5 - watch, 6 - digital tensometric amplifier, a - tensometric mark, b - connector.

The tensometric marks used are of the type 3P/120LY11 manufactured by Hottinger, constant k=2.04±1%. The two tensometric marks were connected in half-bridge and the connector was tied to the tensometric amplifier by a 6-thread cable. The arrow **f** was easily measured in the section a by means of a comparator (5) at all testing stages.

Using the relation Mohr-Maxwell procedure Veresceaghin, the arrow expression becomes:

$$f_A = \frac{Fl_0}{2EI_y}\left[\frac{l_0^2}{3} + \frac{l_1}{2}(2l_0 + l_1)\right] \quad (1)$$

Relation (1) indicates the proportionality between the force **A** and the applied force **F**, or between **fA** (the arrow) and the bending moment $M = \frac{Fl_0}{2}$. Since the beam is subject to pure bending at the middles zone, the tensions σ are proportional to the bending moment (Navier relation).

The proportionality zone on the characteristics curve is highlighted by plotting an arrow curve (f) depending on the specific deformation (ε). From the experimental results, the diagram of the austenite alloyed steel 10TiNiCr180 was plotted in Figure 8.

At the Tensometry Laboratory of ICEPRONAV bending testing were conducted at variable moment. Each sample was installed on a device to the diagram in Figure 9. The samples

were built in at one end while forces of known values were attached to the other end, gradually.

The point for forces application is 100 mm from the central reference of the tensometric mark according to the diagram. The applied forces were obtained with calibrated weigts (order 4) of 0.5 and 1 kgf respectively, which allow for calibrations higher than the accuracy class 0.5. After the experiments and calculations performed the curve in Figure 10 was plotted.

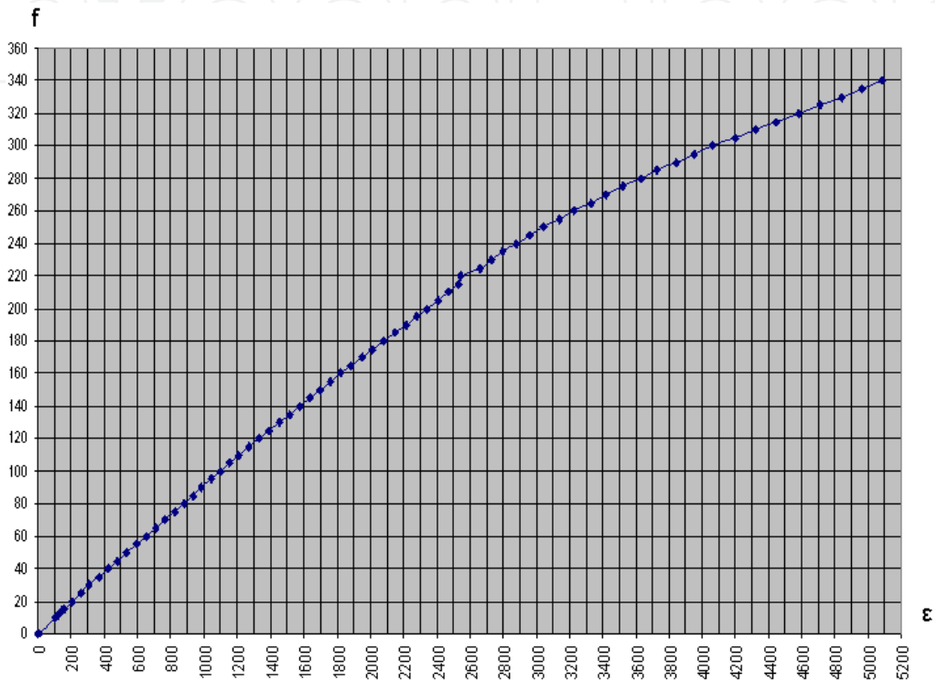

Fig. 8. Pure bending diagram for 10TiNiCr180

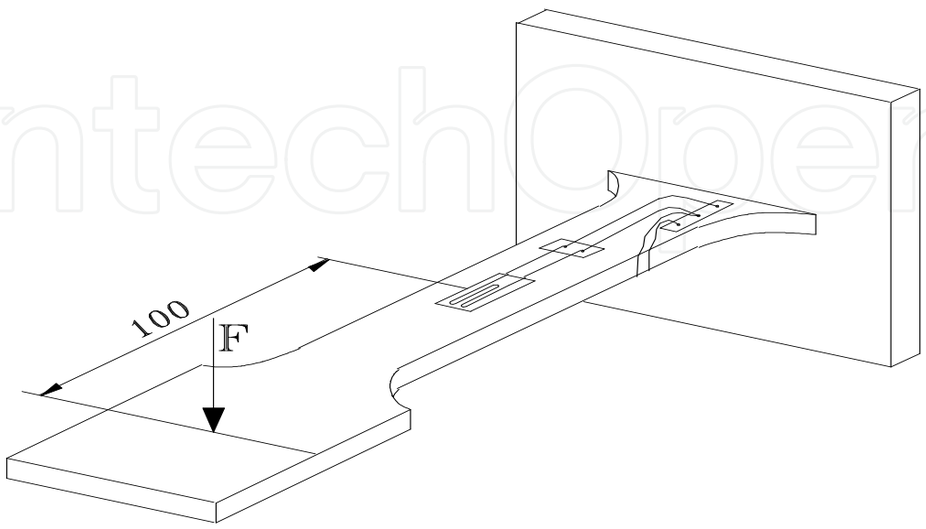

Fig. 9. The sample installed on a device.

It should be underlined that the specific deformations in Figures 9 and 10 are those read on the digital tensometric amplifier N2313; the tensometric marks being connected in half-bridge , $\varepsilon_{real} = \varepsilon_{citit}/2$.

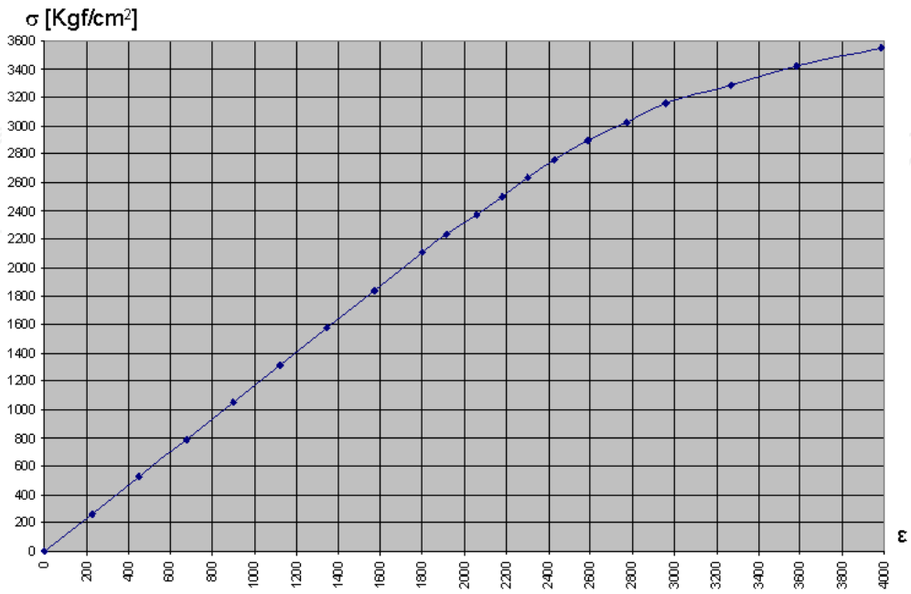

Fig. 10. Bending at variable moment diagram for 10TiNiCr180

From both the experiments and the characterictic curves, three deformations were obtained for the alloyed steel in the transition from the elastic-plastic domain.

The same methodology was used for the carbon steel OL52 and other three deformations were obtained for the above transition domain (according to table 7).

Steel type	Imposed deformations		
	ε_1 [μm/m]	ε_2 [μm/m]	ε_3 [μm/m]
10TiNiCr180	1500	2000	2500
OL52K	2000	2500	3500

Table 7. Imposed deformations in elasto-plastic area.

The values in the table are those recorded while the real ones are half due to the half-bridge arrangement

3.3 The evolution of certain parameters in the surface layer during low cycle fatigue proces

In this chapter the evolution of certain parameters in the surface layer during low cycle fatigue process are presented: evolution of lattice parameter, evolution network parameter, evolution of texture level, variations of microhardness, evolution of microstructures in the surface layer only for ol52 samples tested to pure bending fatigue.

3.3.1 The internal 3rd order strain. The trap density

Figure 11 presents the dependence of $\left(I_f / I_{\max}\right)$ on the number of strain cycles for 3 imposed strains ε_1, ε_2, ε_3 at frequency ν_1= 20 cycles / min for steel OL52.

In general, it is found out the existence of a process of decrease in the trap density in case of small strains (ε_1, ε_2) relative to the original state (level 1 and level 2) and an increase in the trap density (ρ) in case of higher strains ε_3. With increased strain ,a lower degree of deformation of the crystalline lattice around atoms or groups of atoms (dislocation density) is visible.

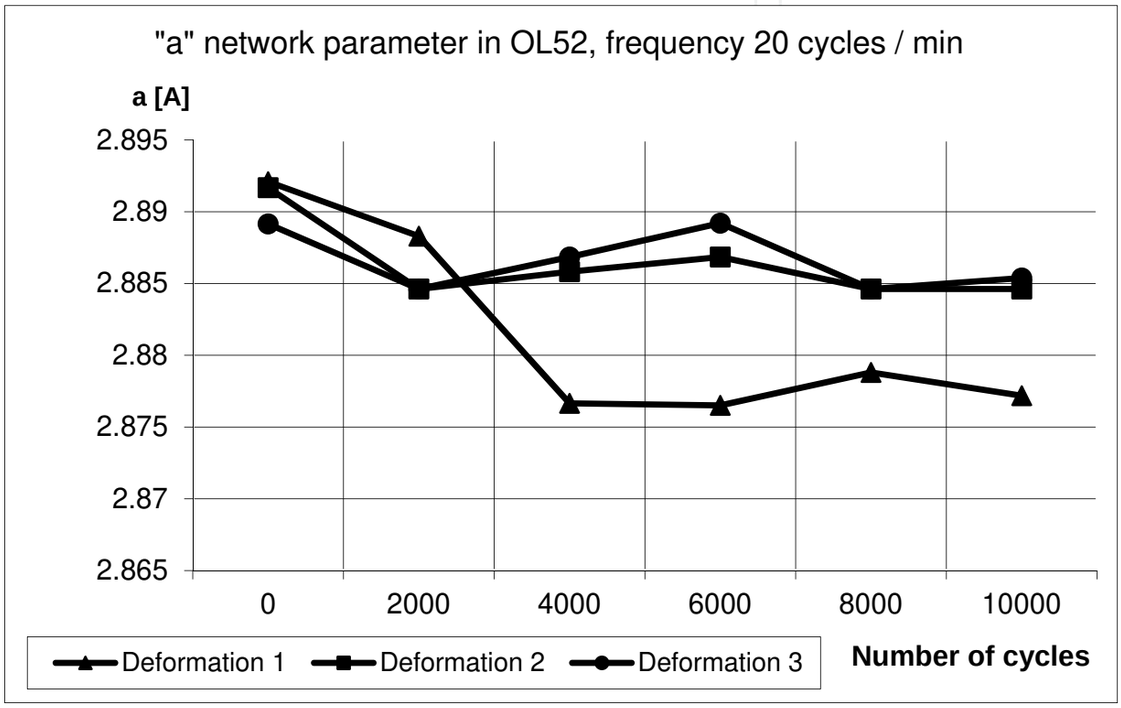

Fig. 11. Evolution of lattice parameter for f = 20 cycles/min

For the average strain ε_2=2500 μm/m it is found a tendency to increase the trap density with the number of strain cycles, said increase taking place in jumps. This increase in the trap density can lead to their agglomeration and subsequently to the generation of micro-cracks. For a strain of ε_1=2000 μm/m the trap density decreases with increasing number of cycles, which can be accounted for by a greater durability of the sample put to strain, when compared with the strain ε_2=2500 μm/m.

As regards the development of the trap densities in the case of strains $\varepsilon_{1=}$ 2000 μm/m and ε_2 = 2500 μm/m, two opposite trends of its variation are found. This may be related to a process of transition from the elastic to elasto-plastic.

With ε_3=3500 μm/m there is a general tendency to increase the trap density, which will hasten the destruction by fatigue as compared with the strain ε_2 = 2500 m / m.

Figure 12 shows the dependence of $\left(I_f / I_{\max}\right)$ on the number of strains for the 3 strain imposed at the frequency of 40 cycles / min for carbon steel OL52.

It is found that for the 3 imposed strains there is an overall decrease in the trap density relative to the initial state.

There is a tendency to increase the trap density with the number of cycles, for the strains of ε_2= 2500 μm / m and ε_3 = 3500 μm/m, and a slight downward tendency of the trap density for a small strain of ε_1=2000 μm/m.

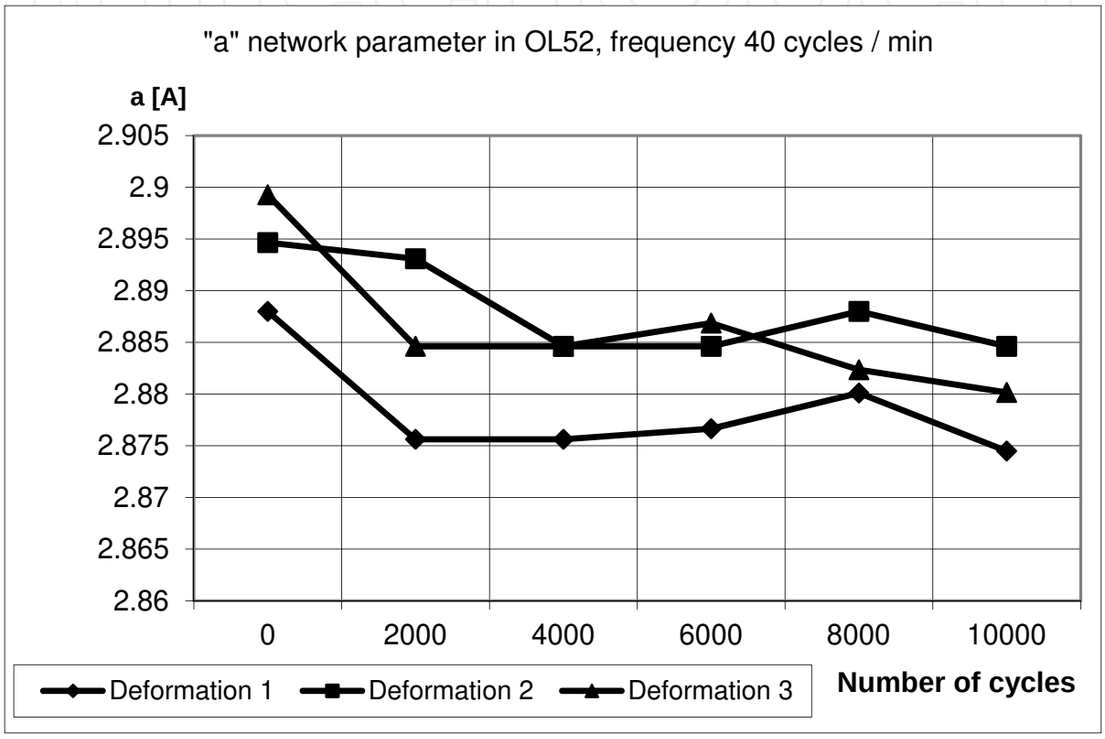

Fig. 12. Evolution of the lattice parameter for f = 40 cycles/min

The downward and upward slopes of the trap density (ε_1=2000 μm/m and ε_2=2500 μm/m) are lower as in the case of frequency of 20 cycles / min above. In addition, the slopes are reversed when compared with the case of frequency of 20 cycles/min.

The fact that there is a change of sign in the slopes at ε_1=2000 μm/m and ε_2=2500 μm/m, again justifies the existence, between the two strains, of a strain of transition from elastic to elasto-plastic.

The trap density variation with the number of cycles has a minimum value the position of which appears increasingly later, as the degree of strain decreases.

From the analysis of the two diagrams it is found that, in order to compensate for the fatigue damage to large strains, high-frequency strains should be applied.

Therefore, at low frequency and large strain, the occurrence of cracks through the process of trap agglomeration is much higher.

3.3.2 Analysis of metallurgical characteristics of the surface layer. Structure analysis. Network parameter

From the analysis of Figures 13 and 14 it is found that the network parameter tends to decrease with increasing number of strain cycles for the 3 strains imposed. The decrease is stronger at small strain and low frequencies and at high frequencies and large strains, respectively. Modification of the network parameter may be associated with the existence of a migration process of the atoms in the alloying elements from the network to the material surface.

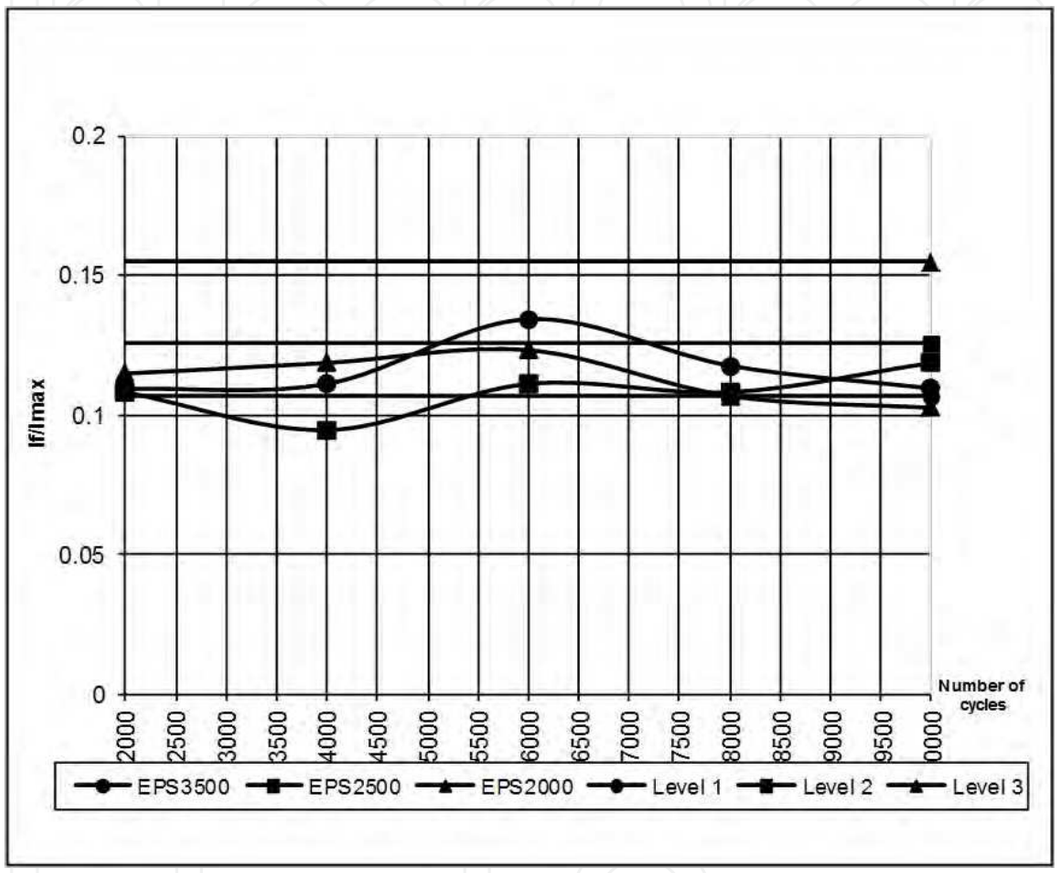

Fig. 13. Variation of the $\left(I_f / I_{\max}\right)_{220}$ on number of testing cycles for frequency v1=20 cycles/min

This is also supported by the slight increase in the network parameter for a given number of cycles. This increase occurs earlier when the strain is greater. The process of atom migration in and from the elementary cell of the ferritic phase indicates a high atom kinetics in the surface layer during the fatigue process.

The high kinetics may have adverse effects if the material would be put to strain in corrosive environments.

Analyzing the two figures it can be seen that the process of atom migration in and from the elementary cell occurs more slowly for low frequencies and faster for high frequencies and large strain; at small strains the process is more pronounced at lower frequencies.

It follows that if the strains were applied in aggressive environments, the life time would be much shorter for low frequencies/low strain and high frequency/ large strains.

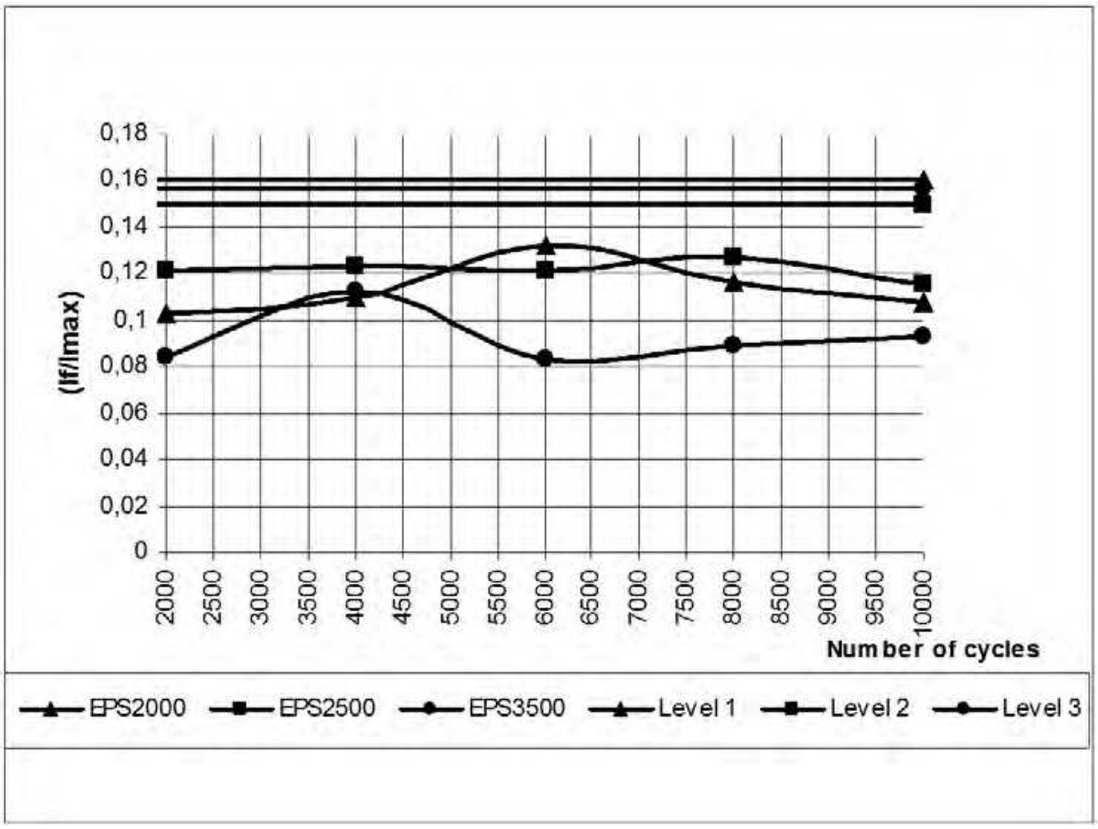

Fig. 14. Variation of the $\left(I_f / I_{\max}\right)_{220}$ on number of testing cycles for frequency ν_1=40

There is therefore the possibility to "manage" from outside the life time by appropriate adjustments of the relationship between the strains imposed and the frequency applied.

3.3.3 Evolution of texture level

Diffractometry investigations with X-rays have highlighted the degree of texturing of OL52 steel sample subjected to high fatigue at the limit of the elastic range and to low frequencies.

As in previous cases, the texture analysis was made in increments of 2,000 cycles to 10,000 cycles and 3 imposed strains. The histogram in Figure 15 shows the dependence of I_{max}/I_0 on the number of cycles N and strain ε, at a frequency of 20 cycles / min.

Analyzing the resulting graphical representation, it is found the predominance of a retexturing process of the material to crystallographic direction (220).

The highest degree of retexturing becomes apparent at the largest strain value, ε_3. This retexturing is associated with the mechanical micro-processes leading to the loss of preferential orientation of crystal planes according to the direction (220) with respect to the state reached after rolling (I_{max}/I_0=1).

With the first strain ε_1, it is found a slight tendency of texturing which increases with increasing number of cycles. With the intermediate strain it is found that there is a stronger texturing which can be associated with the forced orientation of the crystalline planes (220). This material behaviour can be explained by analyzing the first micro processes of elastoplastic strain although, according to the characteristic curve of the material, we found ourselves in the elastic range. Figure 16 provides the histogram of the dependence of $I_{max}/I_{0\ on}$ the number of cycles N and the required strains ε_1, ε_2, ε_3 at the frequency of 40 cycles / min

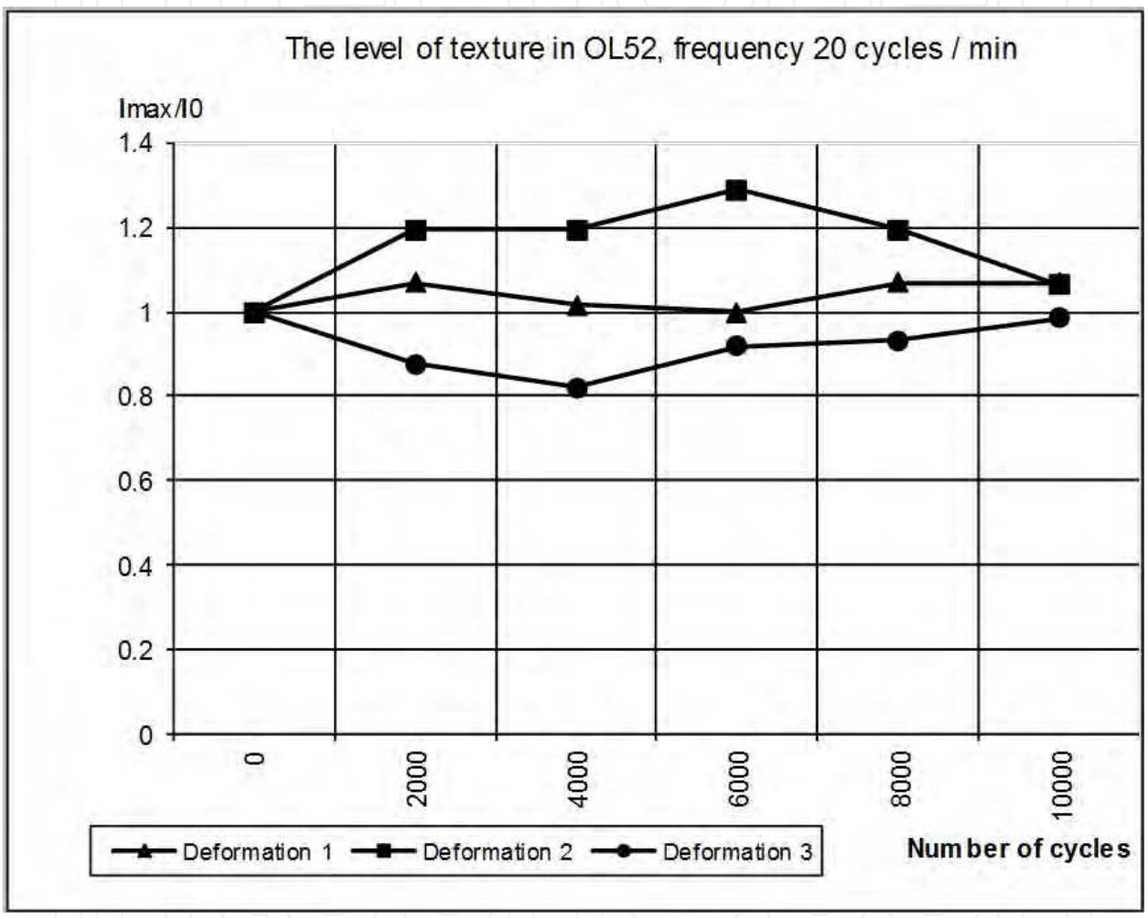

Fig. 15. Evolution of texture level for f = 20 cycles/min

Compared with the previous case, the graphical representation analysis shows that there is a general tendency of increased texture of the crystalline network both with increased number of cycles and the strain required.

With a frequency of 40 cycles / min. no tendency of retexturing was revealed for any amount of strain or number of strain cycles, as in the case described above at a frequency of 20 cycles / min. The fact that at low frequency (ν_1= 20 cycles / min) there are texturing and retexturing processes leads us to the conclusion that the material does not present inertia to changes in structure (hysteresis functions normally), while with high frequency (40 cycles /

min), the material loses part of its elastic properties responding to external factors - inertia to structure changes being much lower.

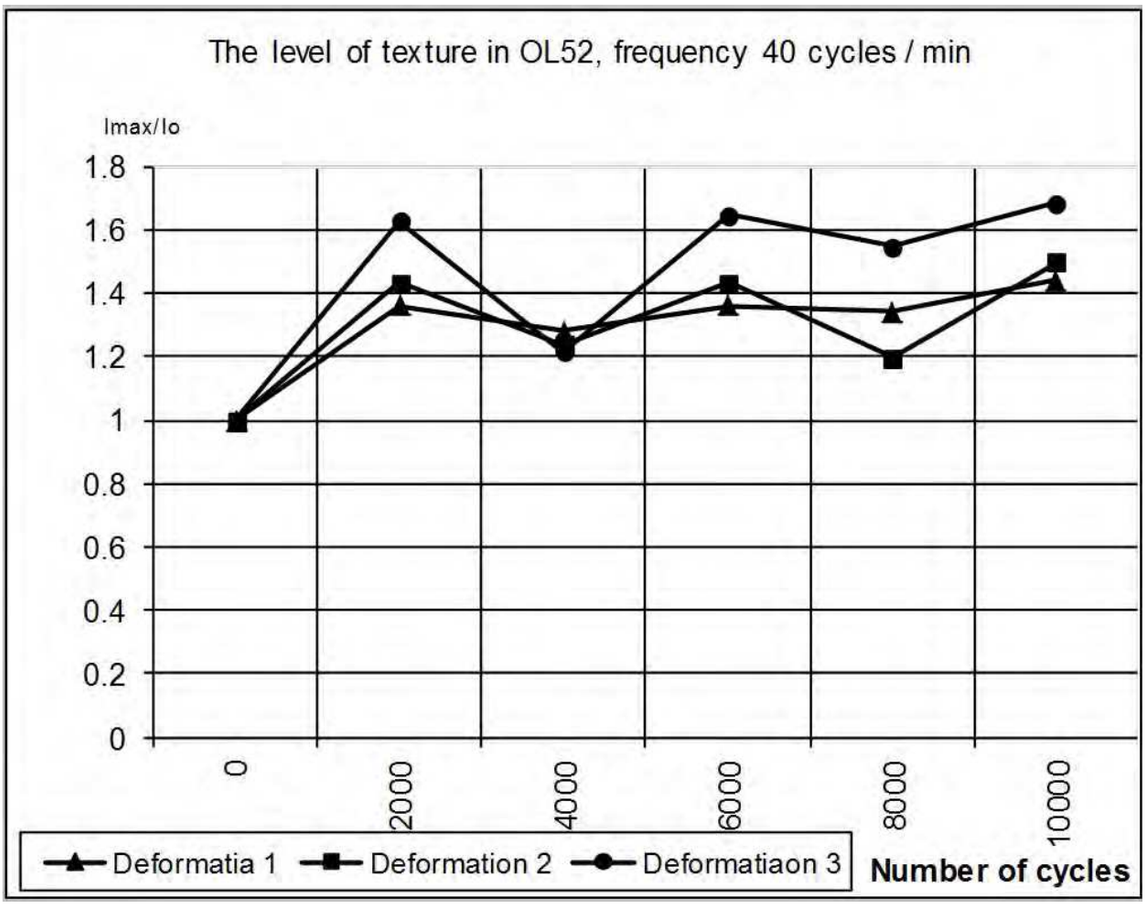

Fig. 16. Evolution of texture level for f = 40 cycles/min

3.3.4 Analysis of the surface layer microhardness

Figure 17 and 18 show the micro hardness HV variation for sample OL52 HV depending on the number of cycles to the strain ε_3=3500 μm/m for the two frequencies. The analysis of the experimental data and curves shows that micro hardness decreases in jumps. The decrease in the micro hardness occurs through processes of hardening and softening. With low frequencies (ν_1=20 cycles/min) decreases in micro hardness is less than the initial state, while at high frequency, the decrease in micro hardness is higher than the initial state. The amplitude of the softening and hardening processes is much higher for low frequencies than for high frequency (ν_2= 40 cycles / min). The period of the hardening and softening processes is lower at low frequencies and higher at higher frequencies. It can be said, therefore, that the velocities of the hardening and softening processes are higher at low frequencies than at higher frequencies for the same strain imposed.

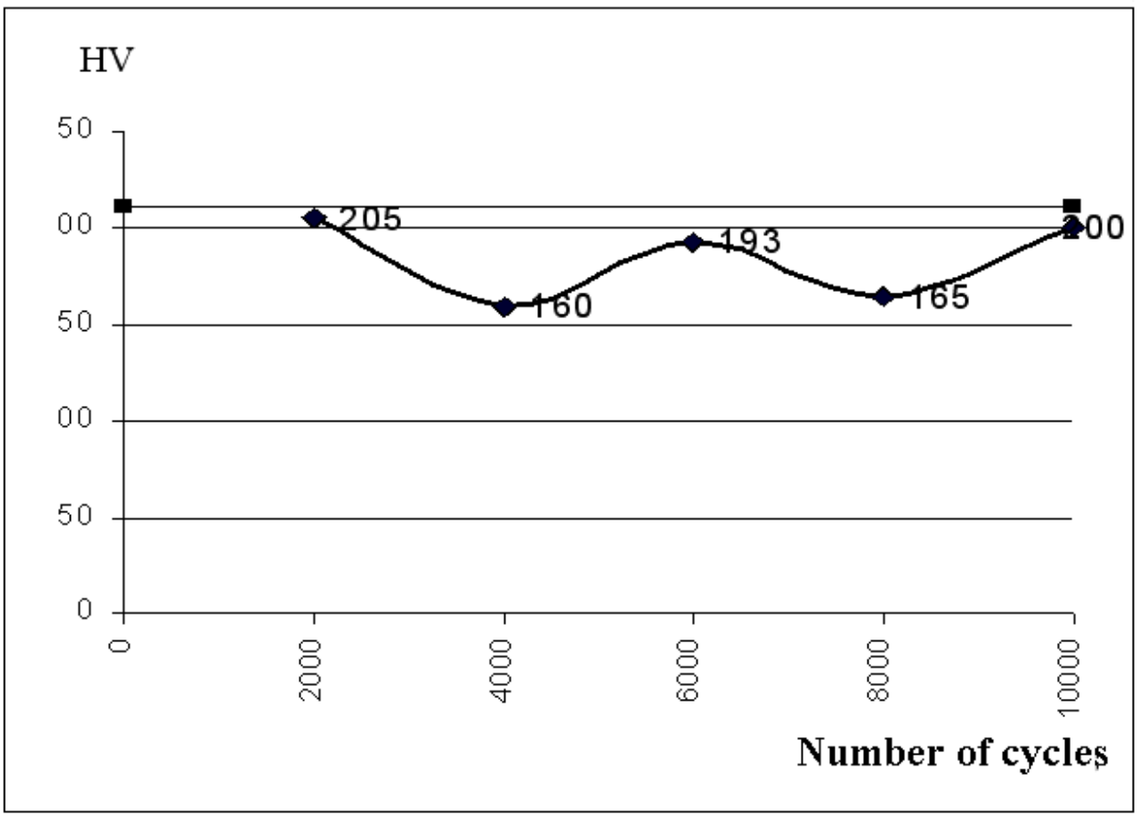

Fig. 17. Variation of microhardness vs testing cycles for v = 20 cycles/min

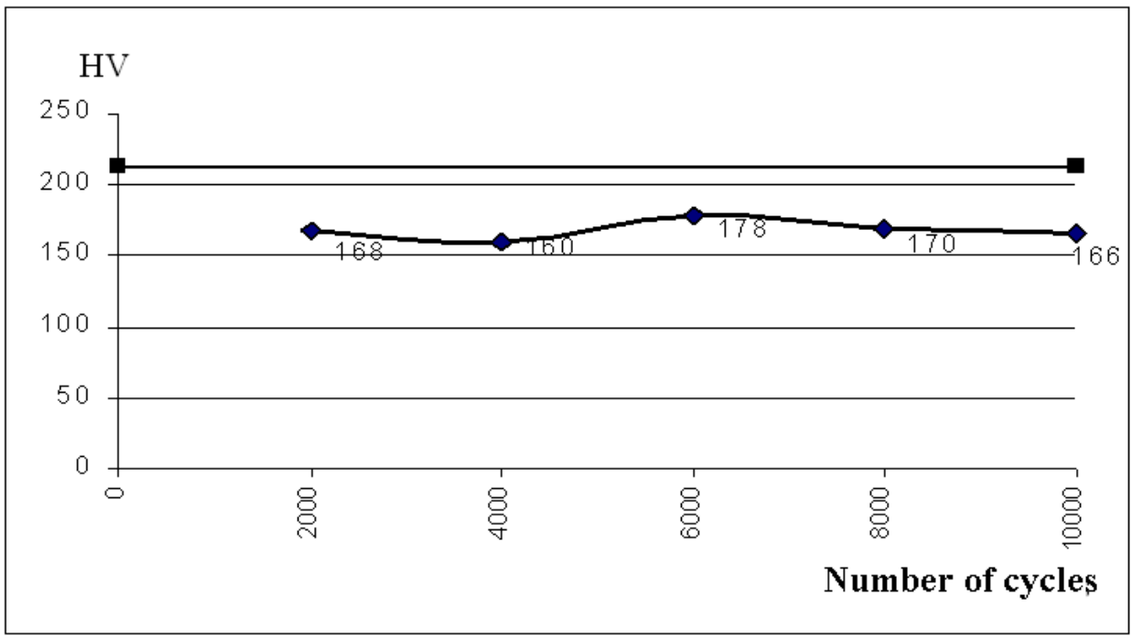

Fig. 18. Variation of microhardness vs testing cycles for v = 40 cycles/min

Number of cycles	x500 v_1=20 cycles/min ε=3500μm/m	x500 v_1=40 cycles/min ε=3500μm/m
Initial state	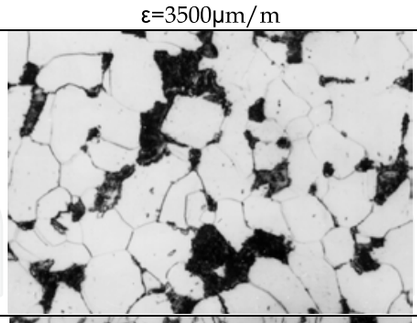	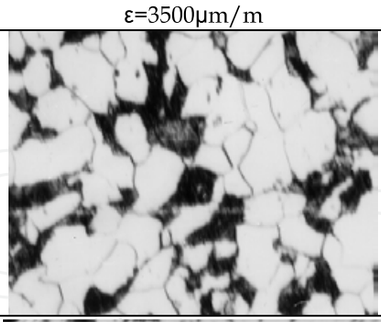
2000	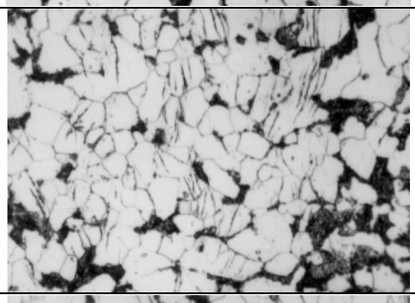	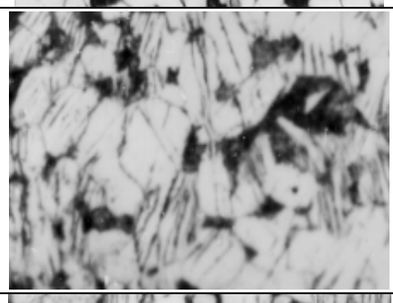
4000	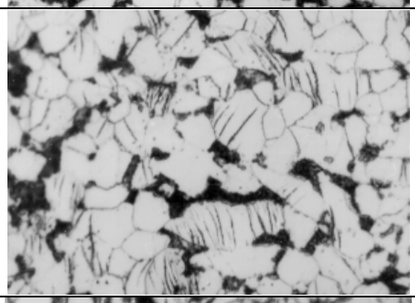	
6000	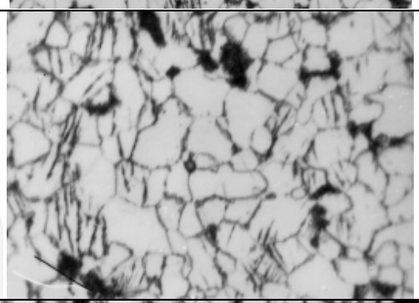	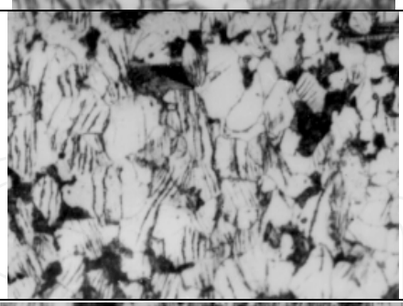
10000	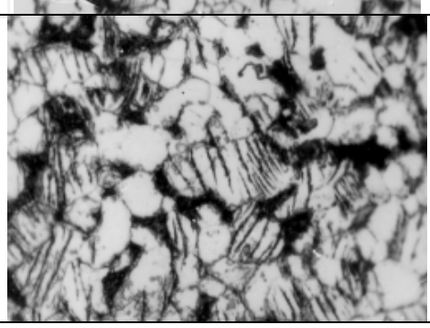	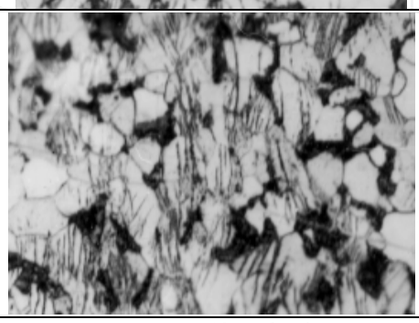
	Fig. 19. v_1=20 cycles/min	Fig. 20. v_1=40 cycles/min

3.3.5 Analysis of microstructure

The microstructure analyses were also carried out in increments of 2,000 cycles up to 10,000 cycles for 3 imposed strains and at the two frequencies (ν_1 şi ν_2).

The Figures 19 and 20 present the microstructures in the surface layer of the OL52 samples tested to pure bending fatigue to the strain ε_3=3500 μm/m, at the two frequencies.

The analysis of the microstructures reveals that with increasing number of cycles there is an increase in the density of the sliding bands in the ferrite grains for a given frequency. With the same strain and number of strain cycles it is observed that with higher frequency the sliding bands density is lower compared with that at lower frequencies.

3.4 Macroscopic aspects of the fractures

Generally, in all cases (Figure 21, 22, 23) the fatigue fracture process is initiated from the sample surface from spots featuring microscopic surface defects (roughness, more intense local hardening because of previous processing, surface defects of the material structure, such as inclusions, intermetallic phases, intersecting the processing surface).

In the section damaged by fatigue process, the samples present a characteristic shiny area and the sudden breaking zone under the strain applied to them.

In case of the sample shown in Figure 23a, on the polished surface near the fracture zone, sliding bands are clearly visible due to the relatively high speed of the strain propagation onto the crystalline grains favorably oriented and of relatively low total hardening intensity. The weight of the plastic strains under elasto-plastic regime is relatively high in a relatively small period of time ((N_{1r} = 30,065 cycles until breaking) to the strain ε_3=3500 μm/m.

The weight of the fatigue fracture surface is relatively small and located near the originator (concentrator) of the breaking/ fracture process (Figure 23b, c).

In Figure 21a, the polished surface reveals sliding bands specific to a very large number of cycles (N_{3r} = 106,488 cycles up to breaking) at a relatively large distance from the break/fracture zone. This indicates that for strains with small strains ((ε_1=2000 μm/m), the elasto-plastic strain zone before fracture is more extensive. The explanation is that the rate of hardening of the material is relatively small and therefore we believe that plastic strains will be taken, at the next cycles, by less hardened neighboring areas which feature lower strain resistance. Extension of the plastic strain area in the vicinity of the fracture zone is accounted for by the propagation of plastic strains, progressively to grains from the neighboring hardened areas.

In Figure 22a, with the sample put to strain ε_2=2500 μm/m, on the polished surface in the vicinity of the breaking zone it is highlighted the presence of sliding bands of highly fine granulation due to the extension of the elasto-plastic range to cover a larger period of time and a larger number of cycles until breaking (N_{2r} = 62,635 cycles). We believe that the weight of plastic strains under elasto-plastic regime is smaller than the previous case.

In Figure 22 b,c the fatigue fracture surface (shiny area) has a relatively greater expansion in the vicinity of the fracture originator and is developed over the entire width of the sample. Both on the previous sample and the sample mentioned above, the fatigue fracture surface is unilateral (on one side).

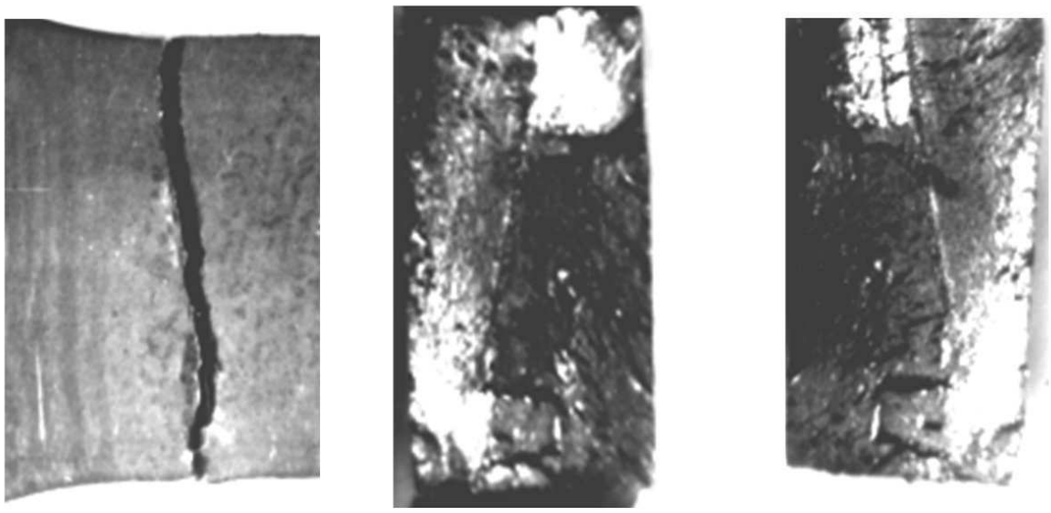

(a) (b) (c)

Fig. 21. Macroscopic aspects of crack for ε_3 = 3500 μm/m

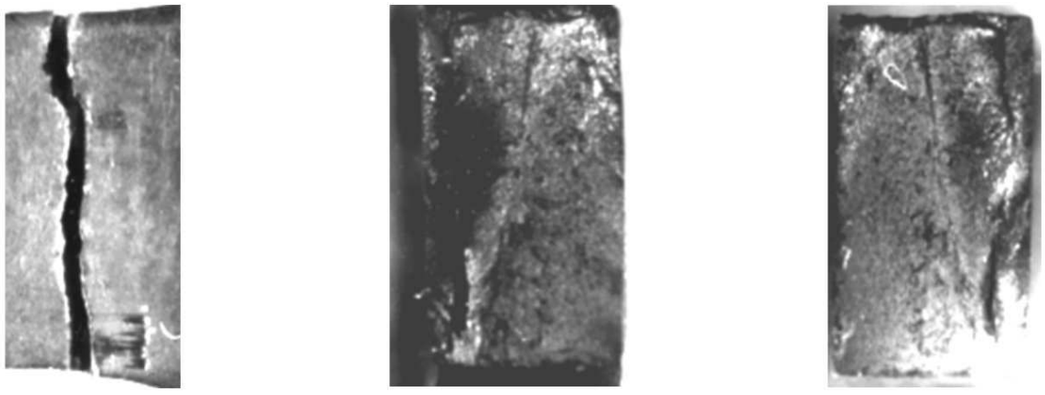

(a) (b) (c)

Fig. 22. Macroscopic aspects of crack for ε_2 =2500 μm/m

(a) (b) (c)

Fig. 23. Macroscopic aspects of crack for ε_1=2000 μm/m

Sliding bands have greater width, this being possible by the accumulation of plastic strain in a relatively large time, i.e. for a larger number of cycles.

In Figure 21b, c, as far as the fracture section is concerned, the fatigue damaged area is much larger than the sudden fracture area, developed over the entire width of the sample, and of bilateral aspect. This can be explained by the fact that the development speed of the fatigue fracture surface from a concentrator is small which allows the initiation of the fatigue fracture from a concentrator on the opposite side.

In the previous cases, since strains are higher, it is sufficient to initiate the fatigue fracture from a stress concentrator because the growth rate of the fatigue fracture is much higher which makes no longer possible the initiation of a fatigue fracture from another concentrator.

4. Conclusions

1. By extension of the tribolayer and tribosystem concepts to the study low cycle fatigue process of the steel the structural changes in the superficial layer are shown. This allows to establish a relationship between structural parameters of superficial layer and damage degree during fatigue tests. It was evinced a microfatigue process which is strong influenced of: frequency testing, strain level, and number of the fatigue tests.
2. Our results can be used to account for the damage mechanism of the tested samples subjected to low frequency fatigue test and high tensions

5. References

Buzdugan, Gh., & Blumenfield, I. (1979), *Calculul de rezistenta al organelor de masini* , Editura Tehnica Bucuresti –Romania, Bucuresti

Constantinescu, I. & Stefanescu, D.M. & Sandu, M., (1989), *Masurarea marimilor mecanice cu ajutorul tensometriei,* Editura Tehnica Bucuresti, ISBN 973-31-0127-3, Bucuresti

Crudu, I.& Macuta, S. & Palaghian, L. & Fazekas L.(1991) "*Masina universala de incercat materiale*", Patent nr. 102714/1991 ,Bucuresti

Gheorghes, C. (1990), *Controlul structurii fine a metalelor cu radiatii X,* Editura Tehnica Bucuresti, ISBN 973-31-0151-6, Bucuresti

Lieurade, H.P. (1982) *La Pratique des Essais de Fatigue,* PYC Editon , ISBN 2-85330-053-6, Paris

Macuta, S. - "*Evolution of some structural fine parameter in the superficial layer during low cycle fatigue process*", Tome I of International Conference on Advanced in Materials and Processing Technologies AMPT'01, vol1.ISBN 84-95821-06-0, Leganes, Madrid – Spania. September 2001

Macuta, S. & Rusu, E., (2008)., Experimental researches regarding the evolution of some parameters of the superficial layer in low cycle fatigue processes ,In: *Maritime Industry Ocean Engineering and Coastal Resources,* Guedes Soares & Kolev, pp. 219 – 223, Taylor and Francis Group , ISBN 978-0-415-45523-7, London

Macuta, S. & Rusu, E., (2009), Experimental researches regarding the evolution of some parameters of the superficial layer in low cycle fatigue processes, *Proceedings of*

13th International Congress International Maritime Association of Mediterranean, tom. 1 - ISBN 978-975-561-356-7, Istanbul Turkey, October 2009

Macuta, S. & Rusu, L., (2009), Modelling by finite element method of stress state establshing and experimental research regarding the elasto-plastic deformations of some steels alloys , *Proceedings of 13th International Congress International Maritime Association of Mediterranean,* tom. 3 - ISBN 978-975-561-358-1, Istanbul Turkey, October 2009

Macuta, S. (2007),. *Oboseala oligociclica a materialelor*, Editura Academiei Romane, ISBN 978-973-27-1382-2, Bucuresti

Macuta, S. (2010) – The Evolution of Certain Parameters In The Surface Layer During Low Cycle Fatigue Process-*Metalugia International Journal* vol.XV Special Issue no.8 , (augusut 2010), pp .20-25 ,ISSN 1582-2214

Macuta, S., (2004)- "*Establishing the elasto-plastic deformations of some steel alloys*", Proceeding of The 29-th Annual Congress of the American Romanian Academy of Arts and Sciences, ISBN 973-632-140-1 Bochum,Germany september 2004.

Mocanu, Ds. (1982), *Incercaera materialelor Vol. 1 & 2,* Editura Tehnica Bucuresti – Romania , Bucuresti

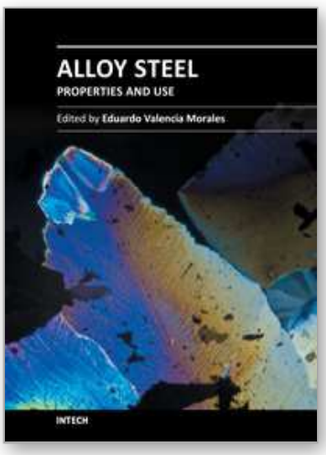

Alloy Steel - Properties and Use

Edited by Dr. Eduardo Valencia Morales

ISBN 978-953-307-484-9
Hard cover, 270 pages
Publisher InTech
Published online 22, December, 2011
Published in print edition December, 2011

The sections in this book are devoted to new approaches and usages of stainless steels, the influence of the environments on the behavior of certain classes of steels, new structural concepts to understand some fatigue processes, new insight on strengthening mechanisms, and toughness in microalloyed steels. The kinetics during tempering in low-alloy steels is also discussed through a new set-up that uses a modified Avrami formalism.

How to reference

In order to correctly reference this scholarly work, feel free to copy and paste the following:

Macuta Silviu (2011). A New Systemic Study Regarding the Behaviour of Some Alloy Steels During Low Cycles Fatigue Process, Alloy Steel - Properties and Use, Dr. Eduardo Valencia Morales (Ed.), ISBN: 978-953-307-484-9, InTech, Available from: http://www.intechopen.com/books/alloy-steel-properties-and-use/a-new-systemic-study-regarding-the-behaviour-of-some-alloy-steels-during-low-cycles-fatigue-process

INTECH
open science | open minds

InTech Europe
University Campus STeP Ri
Slavka Krautzeka 83/A
51000 Rijeka, Croatia
Phone: +385 (51) 770 447
Fax: +385 (51) 686 166
www.intechopen.com

InTech China
Unit 405, Office Block, Hotel Equatorial Shanghai
No.65, Yan An Road (West), Shanghai, 200040, China
中国上海市延安西路65号上海国际贵都大饭店办公楼405单元
Phone: +86-21-62489820
Fax: +86-21-62489821

IntechOpen